

Deep-learning classifier with ultrawide-field fundus ophthalmoscopy for detecting branch retinal vein occlusion

Daisuke Nagasato¹, Hitoshi Tabuchi¹, Hideharu Ohsugi¹, Hiroki Masumoto¹, Hiroki Enno², Naofumi Ishitobi¹, Tomoaki Sonobe¹, Masahiro Kameoka¹, Masanori Niki³, Yoshinori Mitamura³

¹Department of Ophthalmology, Saneikai Tsukazaki Hospital, Himeji 6711227, Japan

²Rist Inc., Tokyo 1530063, Japan

³Department of Ophthalmology, Institute of Biomedical Sciences, Tokushima University Graduate School, Tokushima 7708503, Japan

Correspondence to: Daisuke Nagasato. Department of Ophthalmology, Saneikai Tsukazaki Hospital, 68-1 Waku, Aboshi-ku, Himeji City, Hyogo 671-1227, Japan. d.nagasato@tsukazaki-eye.net

Received: 2018-08-18 Accepted: 2018-12-06

Abstract

• **AIM:** To investigate and compare the efficacy of two machine-learning technologies with deep-learning (DL) and support vector machine (SVM) for the detection of branch retinal vein occlusion (BRVO) using ultrawide-field fundus images.

• **METHODS:** This study included 237 images from 236 patients with BRVO with a mean±standard deviation of age 66.3±10.6y and 229 images from 176 non-BRVO healthy subjects with a mean age of 64.9±9.4y. Training was conducted using a deep convolutional neural network using ultrawide-field fundus images to construct the DL model. The sensitivity, specificity, positive predictive value (PPV), negative predictive value (NPV) and area under the curve (AUC) were calculated to compare the diagnostic abilities of the DL and SVM models.

• **RESULTS:** For the DL model, the sensitivity, specificity, PPV, NPV and AUC for diagnosing BRVO was 94.0% (95%CI: 93.8%-98.8%), 97.0% (95%CI: 89.7%-96.4%), 96.5% (95%CI: 94.3%-98.7%), 93.2% (95%CI: 90.5%-96.0%) and 0.976 (95%CI: 0.960-0.993), respectively. In contrast, for the SVM model, these values were 80.5% (95%CI: 77.8%-87.9%), 84.3% (95%CI: 75.8%-86.1%), 83.5% (95%CI: 78.4%-88.6%), 75.2% (95%CI: 72.1%-78.3%) and 0.857 (95%CI: 0.811-0.903), respectively. The DL model outperformed the SVM model in all the aforementioned parameters ($P<0.001$).

• **CONCLUSION:** These results indicate that the combination of the DL model and ultrawide-field fundus ophthalmoscopy may distinguish between healthy and BRVO eyes with a high level of accuracy. The proposed combination may be used for automatically diagnosing BRVO in patients residing in remote areas lacking access to an ophthalmic medical center.

• **KEYWORDS:** automatic diagnosis; branch retinal vein occlusion; deep learning; machine-learning technology; ultrawide-field fundus ophthalmoscopy

DOI:10.18240/ijo.2019.01.15

Citation: Nagasato D, Tabuchi H, Ohsugi H, Masumoto H, Enno H, Ishitobi N, Sonobe T, Kameoka M, Niki M, Mitamura Y. Deep-learning classifier with ultrawide-field fundus ophthalmoscopy for detecting branch retinal vein occlusion. *Int J Ophthalmol* 2019;12(1):94-99

INTRODUCTION

Branch retinal vein occlusion (BRVO) is a relatively common retinal vascular disorder that causes retinal hemorrhage and macular edema (ME), eventually leading to visual impairment^[1-2]. ME resulting from BRVO is associated with poor visual outcomes^[3-4]. It has been proposed that a delay in the initiation of ME treatment resulting from BRVO affects functional improvement and hinders improvement in visual acuity^[5]. For BRVO, it is important to initiate treatment with antivascular endothelial growth factor agents at an early stage^[5-6]. Treatment of patients at a vitreoretinal center shortly after the onset of BRVO is essential for the preservation of visual function. However, establishing vitreoretinal centers that provide such advanced ophthalmological treatments is impractical considering the associated costs burdening social security schemes of numerous nations worldwide^[7].

Recently, remarkable progress has been achieved in the development of medical equipment, such as the ultrawide-field scanning laser ophthalmoscope (Optos 200Tx; Optos PLC, Dunfermline, United Kingdom) (Figure 1). The Optos system noninvasively provides wide-field fundus images without using a mydriatic agent and is used for the diagnosis, monitoring,

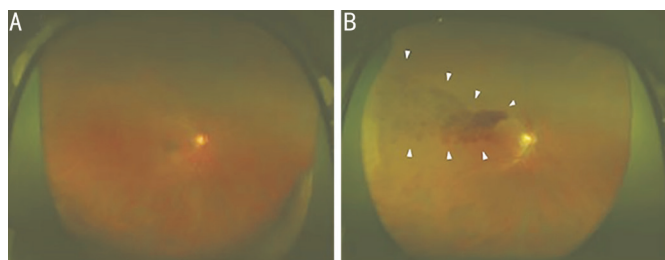


Figure 1 Representative fundus images obtained using ultra-widefield scanning laser ophthalmoscopy A: Ultra-widefield fundus images of the right eye without BRVO; B: Ultra-widefield fundus of the right eye with BRVO. The arrowheads indicate the areas of BRVO.

and treatment of various retinal and choroidal disorders^[8]. If there is no risk of elevation of intraocular pressure due to pupil block after mydriasis, the examiner who is not permitted to administer treatment can acquire the images safely. This is ideal for telemedicine applications in areas where there is no ophthalmologist.

In recent years, image processing approaches using two machine-learning algorithms, namely the deep-learning (DL) and support vector machine (SVM) models, have attracted attention because of their extremely high classification performance. Several studies of their application in medical imaging have been conducted^[9-13]. In ophthalmology, the application of an image processing technology using DL to obtain medical images has been previously reported^[12,14-15]. However, to our knowledge, there have been no studies investigating the automatic diagnosis of BRVO through machine-learning technology using images produced by the Optos system. The aim of this study was to assess the ability of DL and SVM to detect BRVO using Optos images.

SUBJECTS AND METHODS

Ethical Approval This study was conducted in compliance with the principles of the Declaration of Helsinki and was approved by the Ethics Committees of Tsukazaki Hospital and Tokushima University Hospital. Written informed consents were obtained from all subjects for publication of this study and accompanying images.

Data Set Optos image data of patients with BRVO and those without fundus diseases were extracted from the clinical database of the ophthalmology departments of Tsukazaki Hospital and Tokushima University Hospital. These images were reviewed by a retinal specialist for the presence of acute BRVO and registered in an analytical database. Of the 466 fundus images selected, 237 belonged to BRVO patients, while 229 belonged to non-BRVO healthy subjects.

In this study, we used *K*-fold cross validation. This method has been described in detail previously^[16-17]. In brief, the image data were divided into *K* groups. Subsequently, (*K*-1) groups were used as training data and one group was used as validation

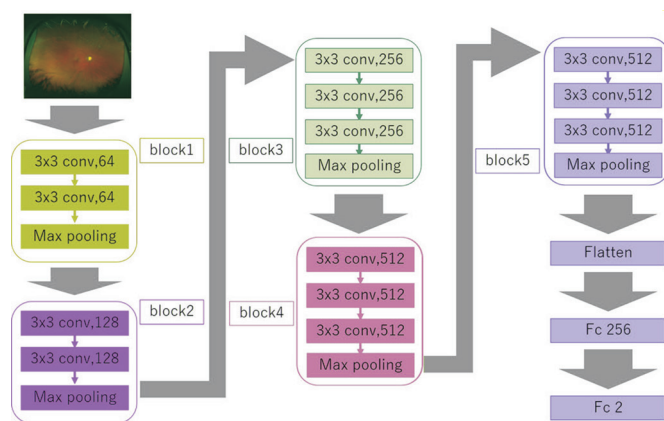


Figure 2 Overall architecture of the VGG-16 model VGG-16 comprises five blocks and three fully connected layers. Each block includes convolutional layers followed by a max-pooling layer. Flattening of the output matrix after block 5 results in two fully connected layers for binary classification. The DNN used ImageNet parameters: the weights of blocks 1-4 were fixed, while the weights of block 5 and the fully connected layers were adjusted.

data. This process was repeated *K* times until each of the *K* groups became a validation data set. The number of groups (*K*) was calculated using Sturges' formula ($K=1+\log_2N$). Sturges' formula is used to decide the number of classes in the histogram^[18-19]. In this study, $1+\log_2237\approx 8.89$ at BRVO, and $1+\log_2229\approx 8.84$ at non-BRVO. So we categorized these two data into nine groups each.

The images of the training data set were augmented through adjustment of brightness, gamma correction, histogram equalization, noise addition, and inversion. Image augmentation increased the amount of learning data by 18-fold. The deep convolutional neural network (DNN) model was created and trained using the data from the preprocessed images.

Deep-learning Model and its Training The DNN model called a visual geometry group-16 (VGG-16)^[20] used in the present study is shown in Figure 2. This type of DNN is known to automatically learn local features of images and generate a classification model^[21-23]. The aspect ratio of the original Optos images was 3900×3072 pixels. For the analysis, we changed the aspect ratio of all input images and resized them to 256×192 pixels. The red-green-blue image input has a range of 0 to 255, so it is normalized into the range of 0-1 by dividing it by 255.

VGG-16 comprises five blocks and three fully connected layers. Each block includes convolutional layers followed by a max-pooling layer decreasing position sensitivity and improving generic recognition^[24]. The flattening of the output of block 5 results in two fully connected layers. The first layer removes spatial information from the extracted feature vectors. The second layer is a classification layer, using the

Table 1 Patient demographics

Parameters	BRVO	Non-BRVO	<i>P</i>
No. of images (patients)	237 (236)	229 (176)	
Age (y)	66.3±10.6	64.9±9.4	0.135 (Student's <i>t</i> -test)
Sex, female (%)	113 (47.9)	84 (47.7)	0.975 (Fisher's exact test)
Left fundus (%)	119 (50.2)	110 (48.0)	0.639 (Fisher's exact test)
Hypertension (%)	131 (55.3)	48 (21.0)	<0.001 (Fisher's exact test)
Diabetes (%)	62 (26.2)	19 (8.3)	<0.001 (Fisher's exact test)
Arterial occlusive disorders (%)	27 (11.4)	11 (4.4)	0.006 (Fisher's exact test)

BRVO: Branch retinal vein occlusion.

feature vectors of target images acquired in previous layers and the softmax function for binary classification. To improve generalization performance, dropout processing was done so that masking was performed with a probability of 25% for the first fully connected layer.

Fine tuning was used to increase the learning speed and achieve high performance even with less data^[25-26]. We used parameters from ImageNet: blocks 1 to 4 were fixed, while block 5 and the fully connected layers were trained.

The weights of block 5 and the fully connected layers were updated using the optimization momentum stochastic gradient descent algorithm (learning coefficient=0.0005, inertial term=0.9)^[27-28]. Of the 40 DL models obtained in 40 learning cycles, the one with the highest rate of correct answers for the test data was selected as the DL model to be evaluated in this study. Keras (<https://keras.io/ja/>) was run on TensorFlow (<https://www.tensorflow.org/>), which is written in the Python programming language, to build and evaluate the model.

Support Vector Machine We used the soft-margin SVM implemented in the scikit-learn library using the radial basis function (RBF) kernel^[29]. We decreased the dimensionality of the images to 60 dimensions. This was the number of dimensions achieving the highest rate of correct answers for the test data (10-70 dimensions in steps of 10 were tested). Optimal values for the cost parameter *C* of the SVM and parameter γ of the RBF were determined through grid search using trifurcation cross validation. The combination with the highest average rate of correct answers was selected. The parameter values for *C* (1, 10, 100, and 1000) and γ (0.0001, 0.001, 0.01, 0.1, and 1) were tested. The final learning model was generated using the optimal parameter values *C*=10 and γ =0.001.

Validation In each split, we calculated the answers of these models for the validation data and we collected the answers for 466 fundus images (237 BRVO images and 229 normal images) from those answers. In each split, training data and validation data are completely separated.

Outcome Receiver operating characteristic (ROC) curves were constructed based on the abilities of the DL and SVM models to distinguish between BRVO and non-BRVO images. These curves were evaluated using sensitivity, specificity,

positive predictive value (PPV), negative predictive value (NPV) and area under the curve (AUC).

Statistical Analysis For comparison of Student's *t*-test was used to compare the age between patients, while Fisher's exact test was used to compare the sex ratio and the ratio of right to left eye images.

The 95%CI of the AUC was obtained as follows. Images judged to exceed a threshold were defined as positive for BRVO, and an ROC curve was constructed. We produced nine models and nine corresponding ROC curves. For AUC, a 95%CI was obtained by assuming a normal distribution and using the average and standard deviation of the nine ROC curves. For sensitivity and specificity, the optimal cutoff values, *i.e.* the points closest to the point at which both sensitivity and specificity are 100% in each ROC curve, were used^[20]. The sensitivities and specificities determined at those cutoff values were used. The ROC curve was calculated using scikit-learn, and the CIs for sensitivity and specificity were determined using scipy. The paired *t*-test was used to compare the AUCs of the DL and SVM models.

Heat Map Images were created by overlaying heatmaps of the DNN focus site on the corresponding BRVO and non BRVO images. A heatmap of the DNN image focus sites was created and classified using gradient-weighted class activation mapping^[30]. The target layer is as the third convolution layer in block 3. The ReLU is represented as `backprop_modifier`. This process was performed using Python Keras-vis (<https://raghakot.github.io/keras-vis/>).

RESULTS

In total, 237 BRVO images from 236 patients (mean age: 66.3±10.6y; 123 males and 113 females; 119 left fundus images and 118 right fundus images) and 229 non-BRVO images from 176 patients (mean age: 64.9±9.4y; 92 males and 84 females; 110 left fundus images and 119 right fundus images) were analyzed. There were no significant differences observed between the two groups in terms of age, sex ratio, or the ratio of right to left eye images. There was a significantly higher rate of hypertension, diabetes and arterial occlusive disorders in the BRVO group than in the non-BRVO group (Table 1).

The sensitivity of the DL model for the diagnosis of BRVO was 94.0% (95%CI: 93.8%-98.8%), the specificity was 97.0% (95%CI: 89.7%-96.4%), the PPV was 96.5% (95%CI: 94.3%-98.7%), the NPV was 93.2% (95%CI: 90.5%-96.0%) and the AUC was 0.976 (95%CI: 0.960-0.993). In contrast, for the SVM model, these values were 80.5% (95%CI: 77.8%-87.9%), 84.3% (95%CI: 75.8%-86.1%), 83.5% (95%CI: 78.4%-88.6%), 75.2% (95%CI: 72.1%-78.3%) and 0.857 (95%CI: 0.811-0.903). In the ROC curves, the AUC of the DL model was significantly better than that of the SVM model ($P < 0.001$; Figure 3).

An image with the corresponding heat map superimposed was produced by the DNN, and the focused coordinate axes in the image were indicated. A representative image is presented in Figure 4. In the image without BRVO, the focal points accumulated around the optic disc. On the other hand, in the image with BRVO, the focal points accumulated around the optic disc and retinal hemorrhages. It is suggested that the DNN may distinguish a BRVO eye from a healthy eye by focusing on the retinal hemorrhages. Blue color was used to indicate the strength of the DNN attention. In the Optos images, the intensity of the color increased on the area of retinal hemorrhages and accumulation was noted at the focus points.

DISCUSSION

In this study, the DL model detecting BRVO through the use of Optos fundus images showed higher sensitivity, specificity, PPV, NPV and AUC than the SVM model. DL is known to automatically recognize the local feature values of images and generate classification models^[21,25,28,31]. Additionally, DL includes several layers for the identification of local features of complicated differences, which can subsequently be combined^[28]. Wang *et al*^[32] reported that the performance of the DL model in the classification of mediastinal lymph node metastases of non-small-cell lung cancer using positron emission tomography/computed tomography images was not significantly different from that of the best standard methods, including SVM and human doctors. In the field of ophthalmology, we previously showed that the DL model using the DNN achieved a better AUC than the SVM model for the detection of rhegmatogenous retinal detachment using ultrawide-field fundus images^[15]. The present study confirmed that the performance of the DL model using the DNN was better than that of the SVM model. This result indicates the possibility of early detection of BRVO through combination of Optos fundus images with DL. Our results demonstrated a classification performance of the DL model that was close to that based on the judgment of an ophthalmologist. At the heat map, the DNN focused around the optic disc in the non-BRVO Optos fundus images and around the optic disc and

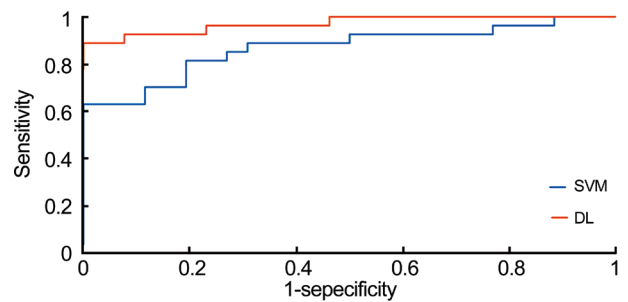


Figure 3 ROC curve of BRVO ROC curve of the nine ROC curves in the DL and SVM models. The AUC of the DL and SVM models were 0.976 and 0.857, respectively. The AUC of the DL model was better than that of the SVM model ($P < 0.001$).

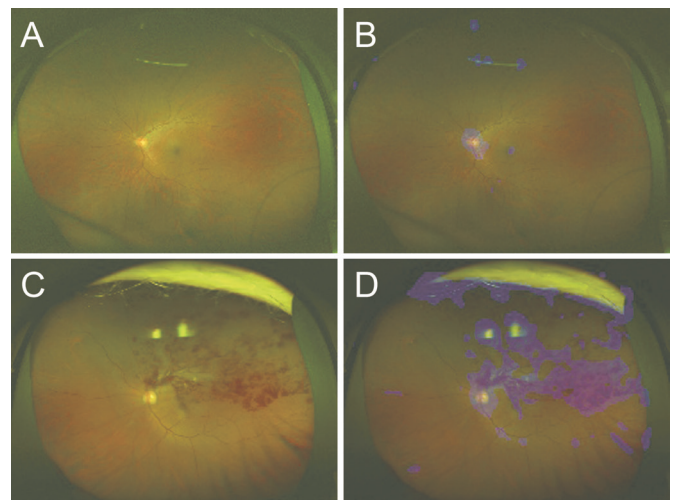


Figure 4 Representative ultrawide-field fundus images and their corresponding heat maps The ultrawide-field fundus image without BRVO (A) and its corresponding heat map (B); with BRVO (C) and its corresponding heat map (D). In the image without BRVO, the deep convolution neural network focused on the optic disc (B; blue color). Meanwhile, in the image with BRVO, the deep convolution neural network focused on the optic disc and retinal hemorrhages (D; blue color).

retinal hemorrhages in the BRVO Optos fundus images. This finding suggests that the proposed DNN model may be useful in diagnosing BRVO by identifying suspected retinal hemorrhages caused by BRVO.

The interpretation of all the acquired Optos fundus photographic images by an ophthalmologist is impractical and costly. However, screening for BRVO may be conducted by non-physician personnel in a nonmydriatic and noninvasive manner using the proposed approach. The combination of the DL model and ultrawide-field fundus ophthalmoscopy is a cost-effective option for the screening and diagnosis of large numbers of patients. This approach may be particularly useful for the diagnosis of BRVO in areas with a shortage or lack of ophthalmic care.

Maa *et al*^[33] reported that tele-ophthalmology has the potential to improve operational efficiency, reduce cost, and significantly improve access to care. In areas with a

shortage of ophthalmological care, the availability of an Optos system offers noninvasive ultrawide-field fundus imaging without requiring the use of a mydriatic agent and avoids the occurrence of complications. The DL technology is able to perform accurate diagnoses of BRVO at a high rate using Optos images. Patients diagnosed with BRVO using this method can immediately consult a retinal specialist and receive the necessary advanced treatment at an ophthalmic medical center. This approach will permit early intervention in BRVO patients residing in medically underserved areas. Moreover, this tele-ophthalmologic technology using Optos may preserve good visual function in BRVO patients residing in areas with inadequate ophthalmic care worldwide.

The following limitations of this study must be acknowledged. Firstly, this study compared only images of health retinas and retinas with BRVO. It did not include images of retinas with other fundus diseases. For an expanded application of this model in the clinical setting, an investigation of other retinal diseases is necessary. Secondly, the analytical ability of Optos is compromised in cases with disorders reducing the clarity of the eye, such as dense cataracts or severe vitreous hemorrhage. Hence, such images were not included in this study. Finally, it is necessary to conduct studies with larger sample sizes and include research on images of other fundus diseases for a more comprehensive evaluation of the performance and versatility of the DL model.

In conclusion, the combination of the DL model and ultrawide-field fundus ophthalmoscopy may distinguish between healthy and BRVO eyes with a high level of accuracy.

ACKNOWLEDGEMENTS

Authors' contributions: Nagasato D wrote the main manuscript text. Tabuchi H, Ohsugi H and Enno H designed the research. Tabuchi H and Mitamura Y conducted the research. Masumoto H performed the DL methods, the SVM methods, and the statistical analysis. Ishitobi N, Sonobe T, Kameoka M and Niki M collected the data. All authors reviewed the manuscript.

Conflicts of Interest: Nagasato D, None; Tabuchi H, None; Ohsugi H, None; Masumoto H, None; Enno H, None; Ishitobi N, None; Sonobe T, None; Kameoka M, None; Niki M, None; Mitamura Y, None.

REFERENCES

1 Rogers S, McIntosh RL, Cheung N, Lim L, Wang JJ, Mitchell P, Kowalski JW, Nguyen H, Wong TY; International Eye Disease Consortium. The prevalence of retinal vein occlusion: pooled data from population studies from the United States, Europe, Asia, and Australia. *Ophthalmology* 2010;117(2):313-319.

2 Bunce C, Xing W, Wormald R. Causes of blind and partial sight certifications in England and Wales: April 2007-March 2008. *Eye (Lond)* 2010;24(11):1692-1699.

3 Kornhauser T, Schwartz R, Goldstein M, Neudorfer M, Loewenstein A, Barak A. Bevacizumab treatment of macular edema in CRVO and BRVO: long-term follow-up. (BERVOLT study: Bevacizumab for RVO long-term follow-up). *Graefes Arch Clin Exp Ophthalmol* 2016;254(5):835-844.

4 Ehlers JP, Kim SJ, Yeh S, Thorne JE, Mruthyunjaya P, Schoenberger SD, Bakri SJ. Therapies for macular edema associated with branch retinal vein occlusion: a report by the American Academy of Ophthalmology. *Ophthalmology* 2017;124(9):1412-1423.

5 Clark WL, Boyer DS, Heier JS, Brown DM, Haller JA, Vittit R, Kazmi H, Berliner AJ, Erickson K, Chu KW, Soo Y, Cheng Y, Campochiaro PA. Intravitreal aflibercept for macular edema following branch retinal vein occlusion: 52-week results of the VIBRANT study. *Ophthalmology* 2016;123(2):330-336.

6 Brown DM, Campochiaro PA, Bhisitkul RB, Ho AC, Gray S, Saroj N, Adamis AP, Rubio RG, Murahashi WY. Sustained benefits from ranibizumab for macular edema following branch retinal vein occlusion: 12-month outcomes of a phase III study. *Ophthalmology* 2011;118(8):1594-1602.

7 Mrsnik M. *Global aging 2013: rising to the challenge*. Standard & Poor's ratings services Network. Available at: https://www.nact.org/resources/2013_NACT_Global_Aging.pdf 2013.

8 Nagiel A, Lalane RA, Sadda SR, Schwartz SD. Ultra-wide field fundus imaging: a review of clinical applications and future trends. *Retina* 2016;36(4):660-678.

9 LeCun Y, Bengio Y, Hinton G. Deep learning. *Nature* 2015;521(7553):436-444.

10 Liu S, Liu S, Cai W, Che H, Pujol S, Kikinis R, Feng D, Fulham MJ, ADNI. Multimodal neuroimaging feature learning for multiclass diagnosis of Alzheimer's disease. *IEEE Trans Biomed Eng* 2015;62(4):1132-1140.

11 Litjens G, Sánchez CI, Timofeeva N, Hermsen M, Nagtegaal I, Kovacs I, Hulsbergen-van de Kaa C, Bult P, van Ginneken B, van der Laak J. Deep learning as a tool for increased accuracy and efficiency of histopathological diagnosis. *Sci Rep* 2016;6:26286.

12 Gulshan V, Peng L, Coram M, Stumpe MC, Wu D, Narayanaswamy A, Venugopalan S, Widner K, Madams T, Cuadros J, Kim R, Raman R, Nelson PC, Mega JL, Webster DR. Development and validation of a deep learning algorithm for detection of diabetic retinopathy in retinal fundus photographs. *JAMA* 2016;316(22):2402.

13 Pinaya WHL, Gadelha A, Doyle OM, Noto C, Zugman A, Cordeiro Q, Jackowski AP, Bressan RA, Sato JR. Using deep belief network modelling to characterize differences in brain morphometry in schizophrenia. *Sci Rep* 2016;6:38897.

14 Gargeya R, Leng T. Automated identification of diabetic retinopathy using deep learning. *Ophthalmology* 2017;124(7):962-969.

15 Ohsugi H, Tabuchi H, Enno H, Ishitobi N. Accuracy of deep learning, a machine-learning technology, using ultra-wide-field fundus ophthalmoscopy for detecting rhegmatogenous retinal detachment. *Sci Rep* 2017;7:9425.

16 Mosteller F, Tukey JW. Data analysis, including statistics. Lindsey G, Aronson E, eds, *Handbook of Social Psychology*, Vol 2, Addison: Wesley;1968.

- 17 Kohavi R. *A study of cross-validation and bootstrap for accuracy estimation and model selection*. Proceedings of International Joint Conference on AI. 1995;1137-1145.
- 18 Maslove DM, Podchiyska T, Lowe HJ. Discretization of continuous features in clinical datasets. *J Am Med Inform Assoc* 2013;20(3):544-553.
- 19 Sturges HA. The choice of a class interval. *Journal of the American Statistical Association* 1926;21(153):65-66.
- 20 Akobeng AK. Understanding diagnostic tests 3: receiver operating characteristic curves. *Acta Paediatrica* 2007;96(5):644-647.
- 21 Deng J, Dong W, Socher R, Li LJ, Li K, Li FF. Imagenet: a large-scale hierarchical image database. *Computer Vision and Pattern Recognition* 2009;248-255.
- 22 Russakovsky O, Deng J, Su H, Krause J, Satheesh S, Ma S, Huang Z, Karpathy A, Khosla A, Bernstein M, Berg AC, Fei-Fei L. Imagenet large scale visual recognition challenge. *Int J Comput Vision* 2015;115(3): 211-252.
- 23 Lee CY, Xie S, Gallagher P, Zhang Z, Tu Z. Deeply-supervised nets. *In AISTATS* 2015;2:5.
- 24 Scherer D, Andreas M, Sven B. Evaluation of pooling operations in convolutional architectures for object recognition. *Artificial Neural Networks* 2010;92-101.
- 25 Redmon J, Divvala S, Girshick R, Farhadi A. You only look once: unified, real-time object detection. 2016 *IEEE Conference on Computer Vision and Pattern Recognition (CVPR)* 27-30 June 2016, Las Vegas, NV, USA, 2016:779-788.
- 26 Agrawal P, Girshick R, Malik J. Analyzing the performance of multilayer neural networks for object recognition. *European Conference on Computer Vision* 2014;329-344.
- 27 Qian N. On the momentum term in gradient descent learning algorithms. *Neural Networks* 1999;12(1):145-151.
- 28 Nesterov Y. A method for unconstrained convex minimization problem with the rate of convergence $O(1/k^2)$. *Doklady AN USSR* 1983;269(27):543-547.
- 29 Brereton RG, Lloyd GR. Support Vector Machines for classification and regression. *The Analyst* 2010;135(2):230-267.
- 30 Akobeng AK. Understanding diagnostic tests 3: receiver operating characteristic curves. *Acta Paediatrica* 2007;96(5):644-647.
- 31 Schisterman EF, Faraggi D, Reiser B, Hu J. Youden Index and the optimal threshold for markers with mass at zero. *Stat Med* 2008;27(2): 297-315.
- 32 Wang HK, Zhou ZW, Li YC, Chen ZH, Lu PO, Wang WZ, Liu WY, Yu LJ. Comparison of machine learning methods for classifying mediastinal lymph node metastasis of non-small cell lung cancer from 18F-FDG PET/CT images. *EJNMMI Research* 2017;7:11.
- 33 Maa AY, Wojciechowski B, Hunt KJ, Dismuke C, Shyu J, Janjua R, Lu XQ, Medert CM, Lynch MG. Early experience with technology-based eye care services (TECS) a novel ophthalmologic Telemedicine initiative. *Ophthalmology* 2017;124(4):539-546.